Development of an Experimental Instrumentation Dedicated to ESD Testing and Measurement on Nanosatellites

Jean-Charles Matéo-Vélez, François Issac, Julien Jarrige, Yoann Bernard-Gardy, Gaël Murat, Jean Guérard, Denis Payan

Development of an Experimental Instrumentation Dedicated to ESD Testing and Measurement on Nanosatellites

Jean-Charles Matéo-Vélez, François Issac, Julien Jarrige, Yoann Bernard-Gardy, Gaël Murat, Jean Guérard, and Denis Payan

***Abstract*— Electrostatic discharges (ESDs) are known to be responsible for satellites anomalies during radiation belts disturbances. Few analyses have been performed so far on nanosatellites however. Ground testing is the most convenient method to evaluate spacecraft charging and its related effects in terms of ESDs and electromagnetic coupling (EMC). This article presents an experimental instrumentation that is fully possible to adapt and embed on nanosatellite mockups.**

***Index Terms*— Electrostatic discharges (ESDs), space vehicles, surface charging.**

I. Introduction

NANOSATELLITES have become very common for the last decade to achieve a large variety of missions (in-orbit demonstration, science, and commercial services). Since the design guidelines for assessing and preventing electrostatic discharges (ESDs) and electromagnetic coupling (EMC) risks [1], [2], [3], [4], [5] have been developed mainly for large platforms, they must probably be adapted to the specificities of smaller platforms, including CubeSats. Low Earth orbit (LEO) charging issues occur in the auroral ovals during auroral electron injections [6], [7]. Geomagnetic substorms are known to increase the ESD risk at geosynchronous (GEO) and middle Earth orbit (MEO) [8], [9], [10], [11]. On the one hand, several factors decrease the surface ESD risks on nanosats. First, their orbits—mostly LEO—are less constraining than GEO and MEO in terms of electron fluxes about a few kiloelectronvolts of energy that are responsible for spacecraft charging. Second, the amplitude and duration of the blow-off (BO) and flash-over (FO) currents are reduced due to a smaller structure and to smaller solar panels. On the other hand, several factors increase the surface ESD risks on nanosats. First, the electronics sensitive to ESD transients and to EMC coupling through the harnesses are closer to the ESD location. Second, there is a relative lack of awareness of nanosatellites and CubeSat designers with respect to more conventional spacecraft.

To better assess ESD and related EMC risks, the BO and FO currents need to be measured with high precision and frequency bandwidth. ONERA and CNES have conducted research and development activities on nanosats charging for a few years. ONERA is currently preparing the CubeSIM payload (sensing impulses and mitigation on CubeSat) for a flight on the ChaRging On CUbeSat satellite (CROCUS) in partnership with Centre Spatial de l'Ecole Polytechnique (CSEP).

Some important issues need to be solved to refine ESD characterization on nanosatellites during ground testing. First, avoid or at least limit any undesired side effects of the test setup on the ESD itself (triggering threshold, current propagation, and absolute potential drop variations). Second, reduce the presence of nearby tank walls and other surfaces to limit their effects on the predischarge electric field, on BO electron trajectories and on the FO plasma expansion. Third, during the discharge, especially during the BO, limit the electrical ringing between the precharged equipment under test and the grounded support equipment (power supplies and capacitor representing the spacecraft capacitance with respect to the space plasma).

The solution adopted in this work is to test as you fly, that is, with an electrically floating mockup. The test setup used in this article is described in a previous paper [12]. It consists of two instruments embedded in a nanosatellite mockup immersed in a vacuum chamber. The current waveforms measured by the first instrument are described in [12]. In this article, we present the results of the second instrument and compare them with the results of the first instrument.

Section II of this article describes the test setup. Section III presents a model of the measurement chain. Section IV presents the test and model results. Section V discusses the applicability of this work to other nanosatellites, and Section VI gives the conclusion and some perspectives.

II. Test Setup

A. Nanosatellite Structural Models

Two nanosatellites mockups have been used. A 2.5U-like structural model (STM) and an 8U-like STM have been manufactured. They are composed of a conductive frame and of metallic plates. Two external panels are mounted on each

Manuscript received 31 August 2022; revised 24 January 2023; accepted 10 March 2023. Date of publication 1 May 2023; date of current version 12 October 2023. This work was supported by the CNES Research and Development Program. The review of this article was arranged by Senior Editor S. T. Lai. *(Corresponding author: Jean-Charles Matéo-Vélez.)*

Jean-Charles Matéo-Vélez, Julien Jarrige, Yoann Bernard-Gardy, Gaël Murat, and Jean Guérard are with the Physics Instrumentation Environment and Space Department, ONERA-The French Aerospace Laboratory, 31055 Toulouse, France (e-mail: Jean-Charles.Mateo_Velez@onera.fr).

François Issac is with the Electromagnetism and Radar Department, ONERA-The French Aerospace Laboratory, 31055 Toulouse, France.

Denis Payan is with the Centre National d´Etudes Spatiales (CNES), Toulouse, France.

Color versions of one or more figures in this article are available at https://doi.org/10.1109/TPS.2023.3262354.

Digital Object Identifier 10.1109/TPS.2023.3262354

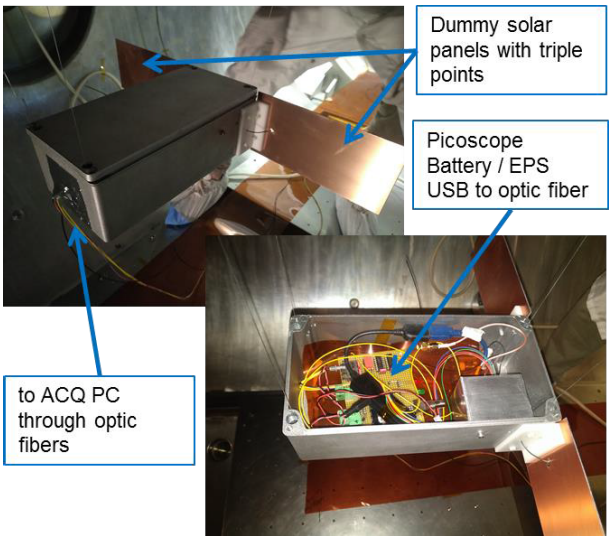

Fig. 1. Pictures of the 2.5U-like nanosatellite STM installed in the JONAS chamber.

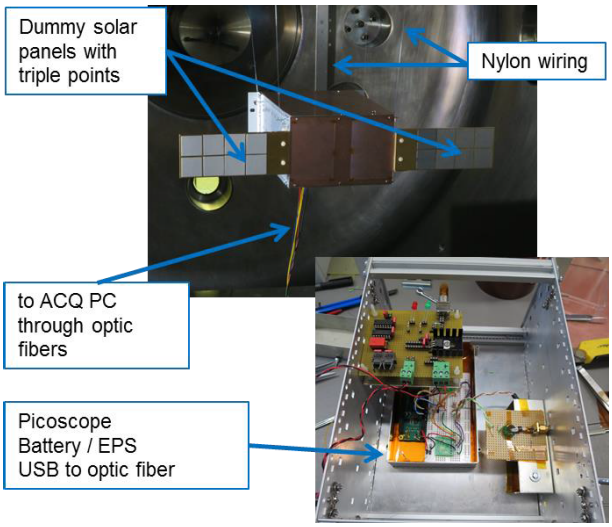

Fig. 2. Pictures of the 8U-like nanosatellite STM installed in the JONAS chamber.

STM to represent deployed solar panels. One side of those deployed panels is conductive. The other side is covered with insulators to mimic solar cell assemblies triple points.

The nanosatellites STM are mounted one at a time at the center of the JONAS vacuum chamber located at ONERA [13]. They are fixed with nylon wires to maintain the electrical insulation with the tank ground. Figs. 1 and 2 show the mockups installed in the vacuum chamber.

B. Instrumentation

Fig. 3 presents the electrical setup installed in each STM. The electronics is powered by an electrical power board and a battery. A picoscope[1] PS4227 is connected to the laboratory acquisition system through an optical fiber. This scope maintains the electrical insulation of the mockup with respect to the tank ground. Channel 1 of the scope is connected to a 4.7-Ω

[1]Registered trademark.

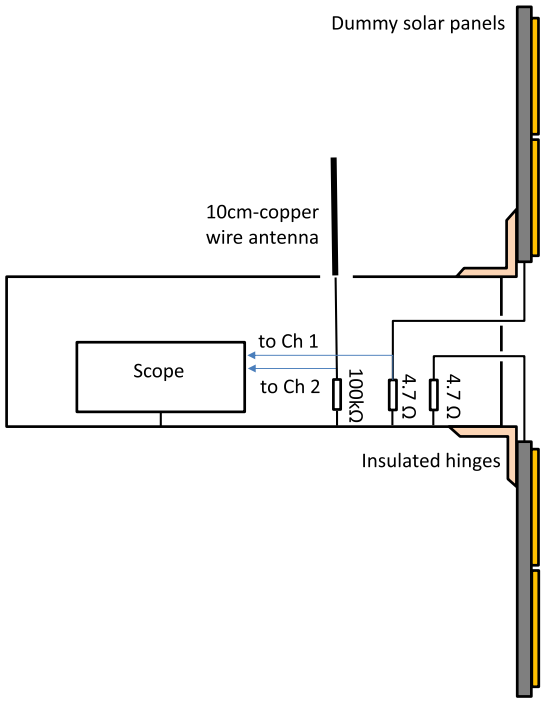

Fig. 3. Electrical setup installed in the nanosatellite STM.

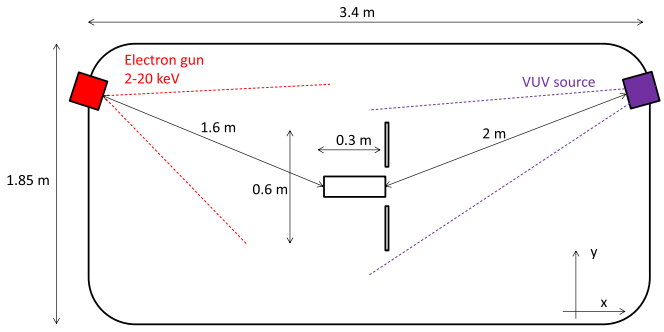

Fig. 4. Charging conditions inside the JONAS chamber.

resistor load connecting one external panel to the STM frame. That external panel is referred as the instrumented panel in this article. The other one is referred as the noninstrumented panel. A Pearson probe has also been used instead of the resistor to measure the current flowing between the panel and the frame. Channel 2 detects the electrical potential variations associated with ESDs. It is connected to the terminals of a 100-kΩ resistor placed between the frame and a 10-cm-long conducting wire. This wire antenna is located outside and perpendicularly to the STM.

C. Charging Conditions

Fig. 4 presents the conditions used to charge the nanosatellites STM. An electron gun produces an electron beam with energy from 5 to 15 keV and a current density from 0.1 up to 10 nA/cm^2. The electron beam makes the STM frame charge negative with respect to the ground.

A vacuum ultra-violet (VUV) source illuminates the opposite side mostly covered with insulators. The photons eject

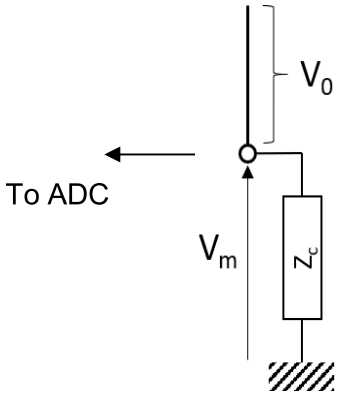

Fig. 5. Antenna measurement schematical representation.

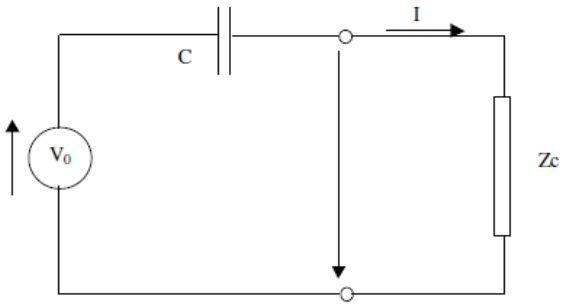

Fig. 6. Antenna measurement equivalent electrical circuit.

electrons through photoemission. This produces the so-called inverted potential gradient (IPG) situation with negatively charged conductors and less negatively charged insulators at the triple points located on the external panels. This is known to facilitate surface ESDs. All tests have been performed with both the electron gun and the VUV source.

III. Measurement Modeling

The antenna measurement physical principle is sketched in Fig. 5, where Z_c is the load 100-kΩ resistor. The antenna voltage V_0 is proportional to the local electric field E

$$V_0 = -l_{\text{eq}} \times E$$

where l_{eq} is the antenna equivalent length.

E is assumed to be proportional to the nanosatellite mockup frame potential V_{sat}

$$E = k \times V_{\text{sat}}$$

where k is a constant that depends on nanosatellite geometry.

During an ESD, the satellite voltage evolves with the BO current I_{BO} according to the following equation:

$$C_{\text{sat}} \times dV_{\text{sat}}/dt = I_{\text{BO}}$$

where C_{sat} is the nanosatellite capacitance with respect to the ground.

The equivalent circuit of the antenna measurement is a high pass (see Fig. 6), where C is the antenna capacitance with respect to the nanosatellite frame.

The relation between the antenna voltage and the measurement output V_m is

$$V_m = \frac{1}{1 + \frac{1}{jZ_cC\omega}} V_0.$$

For a signal with a characteristic frequency higher that the high pass cutoff frequency, the output voltage V_m tends to V_0. In this limit, the antenna signal simply writes

$$\frac{dV_m}{dt} = kl_{\text{eq}} \frac{I_{\text{BO}}}{C_{\text{sat}}}.$$

According to the Gauss theorem, we concluded that the BO current can be computed from the shunt resistor current, from the size of the different surfaces (platform and panels) and from the ESD location [12]

$$I_{\text{BO}} = \alpha_1 \times I_{\text{shunt}}, \quad \text{with } \alpha_1 = 15/13 \text{ for the tested model.}$$

When the ESD occurs on the instrumented panel, with I_{shunt} the current measured on the shunt resistor of the instrumented panel and α_1 a constant, and

$$I_{\text{BO}} = -\alpha_2 \times I_{\text{shunt}}, \quad \text{with } \alpha_2 = 15/2 \text{ for the tested model}$$

when the ESD occurs anywhere else. The parameters l_{eq}, k, C_{sat}, α_1, and α_2 are constants that depend on the spacecraft dimensions and of materials arrangements.

IV. Results

A total number of 87 ESDs and 43 ESDs have been measured on the 2.5U and 8U mockups, respectively. The current waveforms are presented in [12]. In the following, we focus on the 27 ESDs obtained on the 8U mockup panels made of alumina plates glued on a gold-coated aluminum plate and under an electron beam of energy from 6 to 9 keV and current density of 5 nA/cm^2. We checked the ESD position with a video camera. The electrical signal quality is very good, with high precision and very limited current ringing. The current is clearly split into two phases. The first phase lasts from 0.5 to 1.5 μs. This is the BO current that discharges the STM negative potential with respect to the tank ground. The second phase concerns the development of an FO current that reduces the relatively positive voltage of surface insulators impacted by VUV. We checked this by measuring the surface potential on external panels before and after the ESDs with a contactless voltage probe. The FO current lasts often longer than 10 μs on both 2.5U and 8U mockups.

Fig. 7 shows an example of the transient signals measured for an ESD that occurred on the instrumented panel during a discharge with an FO lasting more than the acquisition time period of 4 μs. The shunt resistor current reaches 200 mA. The antenna voltage rises up to 15 V in absolute value. Both signals are well correlated.

Fig. 8 presents the duration of the BO current as derived from the antenna signal and from the shunt current. The BO phase, which corresponds to the discharge of the satellite with respect to the environment, is characterized by a peak-shaped ESD current with a fast transient. The FO phase, which corresponds to neutralization of charges between the different parts

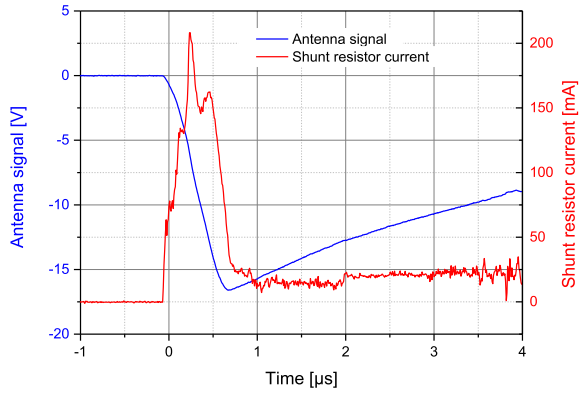

Fig. 7. Example of transient signals measured during an ESD.

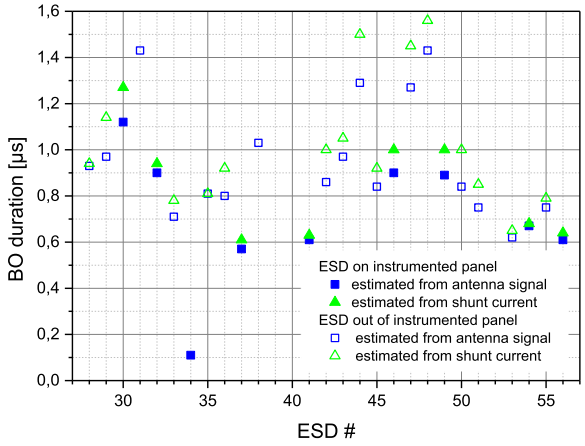

Fig. 8. BO duration derived from the antenna signal and from the shunt current on the 8U-like mockup.

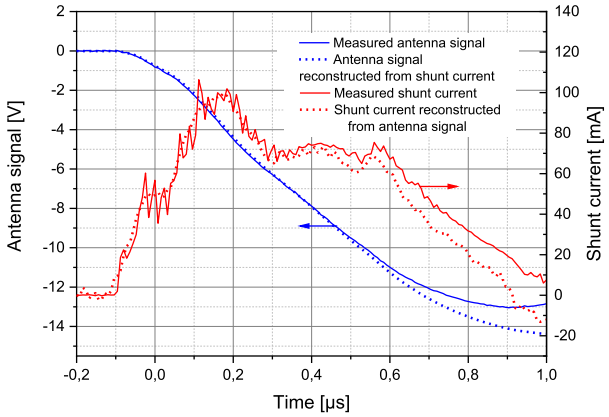

Fig. 9. Antenna and shunt signals measured during an ESD that occurred on the instrumented panel, compared with the antenna signal reconstructed from the measured shunt current and with the shunt current reconstructed from the antenna signal.

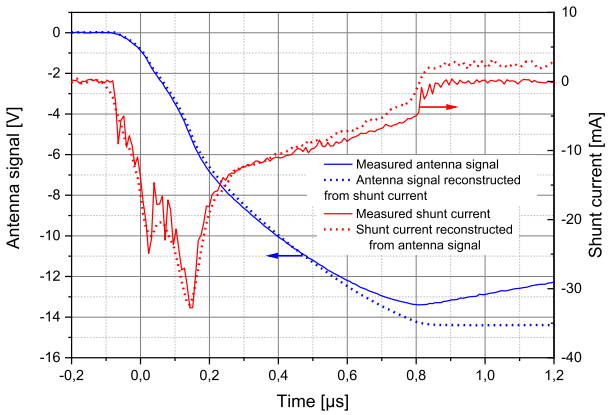

Fig. 10. Antenna and shunt signals measured during an ESD that occurred on the noninstrumented panel, compared with the antenna signal reconstructed from the measured shunt current and with the shunt current reconstructed from the antenna signal.

of the satellite (dielectric surfaces and conductive structure), is characterized by a steady ESD current. Hence, the BO duration can be inferred from shunt resistor current at the transition between the two phases. Concerning the antenna, the BO duration is estimated from the derivative of the signal ($dV_m/dt = 0$ at the end of the BO).

In the example of Fig. 7, the estimated BO duration is about 0.67 and 0.68 μs using the antenna and the shunt resistor, respectively. Overall, the BO duration measured in this test campaign ranges from 0.5 up to 1.5 μs with no difference on whether the ESD occurs on the instrumented panel or elsewhere.

Figs. 9 and 10 present the signals measured on the antenna during two ESDs that occurred on different places, i.e., one on the instrumented panel and the other one on the noninstrumented panel. As expected, the shunt current has opposite sign. The measured current amplitude is larger on ESDs occurring on the instrumented panel. On these plots, time zero is a bit after the start of the discharge because of oscilloscope trigger settings.

The secondary peak observed in Fig. 9 is not a specificity of ESDs occurring on the instrumented panel. We have observed secondary peaks on some ESDs occurring out of the instrumented panel, and we have observed as well waveforms with a single peak for ESDs occurring on both the instrumented panel and elsewhere.

The analysis of the 27 ESDs showed that the above model is well satisfied with the following parameterizations:

$$k \times l_{\text{eq}} \times \alpha_1 / C_{\text{sat}} = 2.33 \times 10^8 F^{-1} \text{ and}$$
$$k \times l_{\text{eq}} \times \alpha_2 / C_{\text{sat}} = 1.3 \times 10^9 F^{-1}.$$

These numbers have been derived by fitting the shunt resistor current reconstructed from the antenna signal with the actual measured current. The model is illustrated in Figs. 9 and 10 that represent the time evolution of the measured signals compared with the signals computed from the model, i.e., the antenna signal reconstructed from the measured shunt current and the shunt current reconstructed from the measured antenna signal. The fine structures in the antenna signal are not all visible in the plots, but they explain the fine structure of the reconstructed shunt resistor current. However, one can notice as expected that the structures of the measured shunt resistor current are finer than those of the reconstructed one.

The ratio between α_1 and α_2 is close to the ratio of 1/6 between the surfaces of the instrumented panel and of the

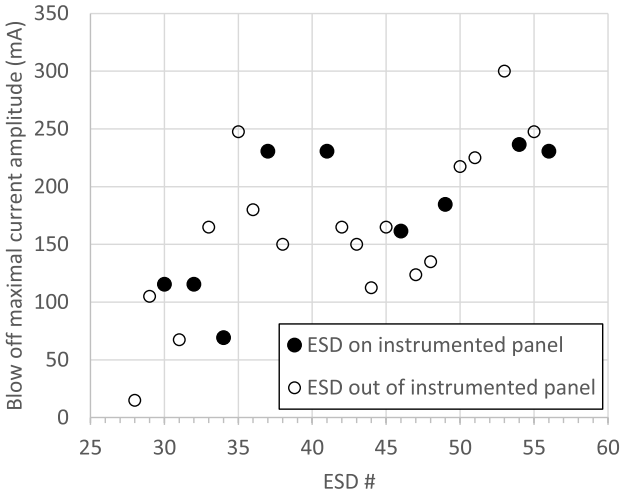

Fig. 11. BO maximal current amplitude derived from the shunt current on the 8U-like mockup.

other surfaces. To reconstruct the BO amplitude, we are thus tempted to follow our previous analysis and to use the factor of 15/13 for α_1 and 15/2 for α_2 derived from the Gauss theorem [12]. Fig. 11 presents the maximal BO current amplitude as derived from the shunt resistor with an average of 170 mA and a standard deviation of 70 mA. The bottom and upper limits are 15 and 300 mA. The differences are believed to be induced either by different absolute spacecraft potential just before the ESD and/or by some damping effects reducing the development of the cathode spot.

V. Discussion

The benefit of testing ESDs on full nanosat mockups is to assess the characteristics of ESDs whatever their position and possibly their effects on electronics boards if present as well inside the mockup. The nanosatellites dimensions are compatible with full-size and floating tests. For space missions with a large spacecraft, only a few coupons can be tested and a component capacitor is added to the coupon to represent the missing parts with unavoidable side effects on the electrical circuit as demonstrated in our previous paper [12]. The question is now to know whether new tests with other nanosatellite mockups would give different results. The variations in the BO currents and durations presented in this article and in the previous paper can be explained by many reasons including the onset absolute voltage at ESD ignition, the location of the triple points, and the charging conditions. We have focused on Geo-like conditions with high fluxes of high energy electrons and VUV. One could argue that the results could be very different for a nanosatellite of different dimensions and surface materials that would fly in LEO polar orbit, for instance. Any change in the mission profile could lead to different test results and using a full-scale mockup with both representative electrical circuit and surface materials only will allow a proper assessment of the in-rush current flowing through harnesses and electrical components. All this reinforces the need to build a database of ESD characteristics on nanosatellite mockups to help the community prepare against the ESD hazard.

VI. Conclusion

The test setup developed in this work is well suited to characterize ESD on nanosatellites because the electrical noise and disturbance are very limited by the disconnection between the tank ground and the mockups. No signal filtering is required. The BO peak current ranges from 15 to 300 mA with an average of 170 mA and standard deviation of 70 mA. Its duration ranges from 0.5 to 1.5 μs under the test conditions presented in this article. The contactless surface potential probe could possibly be used to get the absolute potential just before an ESD occurs but some care would be required not to modify the charging process by masking VUV, nor the transients signal by modifying the absolute spacecraft capacitance for instance.

The energy released is in the order of a few tens of micro-Joule, assuming a voltage drop of 1000 V and a capacitance of a few hundreds of picofarad, which is enough to trigger bitflips in electronics. In addition, cable lengths on nanosatellites are significantly smaller than on more conventional spacecraft that results on much less resistive and inductive losses on the path from the ESD site to the sensitive electronics. In many cases, cables on nanosats are less shielded. All this would suggest re-evaluating the risks with regard ESD/EMC.

The sensors used in this study are good candidates for in-flight ESD detection and waveforms measurements with reasonable bandwidth (10–100 MHz) pending on nanosatellite specifications in terms of allocated power and data budget. It is quite easy to adapt these techniques to any nanosatellites mockups with their specificities (size, materials, electrical circuit, and environmental conditions). The cross-calibration of the antenna and current measurement must be done with nanosatellites mockup representative of the flight models because their parameters are geometry dependent. It has been shown that the BO current could be reconstructed from the antenna signal only.

Additional sensors are under investigation to evaluate the predischarge absolute nanosat potential and FO propagation. We plan to test miniaturized sensors embedded in the CubeSIM payload, currently in phase C, and to fly them on the CROCUS mission, currently in phase B.

Acknowledgment

The CubeSIM/CROCUS project is supported by the ONERA ONSAT-1 Research Program. The authors thank the CROCUS team members at ONERA and at CSEP. They are grateful to helpful discussions with Laurent Garrigues from LAPLACE laboratory in Toulouse.

References

[1] C. K. Purvis, H. B. Garrett, A. C. Whittlesey, and N. J. Stevens, "Design guidelines for assessing and controlling spacecraft charging effects," NASA, Washington, DC, USA, Tech. Paper NAS 1.60: 2361, 1984. [Online]. Available: https://ntrs.nasa.gov/citations/19840025381

[2] National Aeronautics and Space Administration. (2022). *Mitigating in Space Charging Effects—A Guideline (NASA Standards NASA-HDBK-4002B)*. [Online]. Available: https://standards.nasa.gov/standard/nasa/nasa-hdbk-4002

[3] European Cooperation for Space Standardization. (2019). *Spacecraft Charging (ECSS Standard ECSS-E-ST-20-06C)*. [Online]. Available: https://ecss.nl/standard/ecss-e-st-20-06c-rev-1-spacecraft-charging-15-may-2019

[4] International Organization for Standardization (2011). *Space Systems Space Solar Panels Spacecraft Charging Induced Electrostatic Discharge Test Methods (ISO 11221:2011)*. [Online]. Available: https://www.iso.org/standard/50296.html

[5] European Cooperation for Space Standardization. (2019). *Assessment of Space Worst Case Charging Handbook (ECSS Standard ECSS-E-HB-20-06A)*. [Online]. Available: https://ecss.nl/home/ecss-e-hb-20-06a-assessment-of-space-worst-case-charging-handbook-15-may-2019.

[6] P. C. Anderson, "Characteristics of spacecraft charging in low Earth orbit," *J. Geophys. Res., Space Phys.*, vol. 117, no. A7, Jul. 2012, Art. no. A07308, doi: 10.1029/2011JA016875.

[7] A. I. Eriksson and J. E. Wahlund, "Charging of the Freja satellite in the auroral zone," *IEEE Trans. Plasma Sci.*, vol. 34, no. 5, pp. 2038–2045, Oct. 2006, doi: 10.1109/TPS.2006.883373.

[8] J. F. Fennell, H. C. Koons, J. L. Roeder, and J. B. Blake, "Spacecraft charging: Observations and relationship to satellite anomalies," Aerosp. Corp., Defense Tech. Inf. Center Rep., Aerosp. Rep. TR-2001 (8570)-5. [Online]. Available: https://apps.dtic.mil/sti/citations/ADA394826

[9] P. C. Anderson and H. C. Koons, "Spacecraft charging anomaly on a low-altitude satellite in an aurora," *J. Spacecraft Rockets*, vol. 33, no. 5, pp. 734–738, Sep. 1996, doi: 10.2514/3.26828.

[10] D. Ferguson, W. Denig, and J. Rodriguez, "Plasma conditions during the galaxy 15 anomaly and the possibility of ESD from subsurface charging," in *Proc. 49th AIAA Aerosp. Sci. Meeting including New Horizons Forum Aerosp. Expo.*, Jan. 2011, p. 1061, doi: 10.2514/6.2011-1061.

[11] N. Ahmad, D. Herdiwijaya, T. Djamaluddin, H. Usui, and Y. Miyake, "Diagnosing low Earth orbit satellite anomalies using NOAA-15 electron data associated with geomagnetic perturbations," *Earth, Planets Space*, vol. 70, no. 1, p. 91, Dec. 2018, doi: 10.1186/s40623-018-0852-2.

[12] Y. Bernard-Gardy et al., "Innovative technique for electrostatic discharges characterization on a floating nanosatellite mockup," *J. Spacecraft Rockets*, vol. 60, no. 1, pp. 172–180, Jan. 2023.

[13] J.-C. Mateo-Velez, J.-F. Roussel, D. Sarrail, F. Boulay, V. Inguimbert, and D. Payan, "Ground plasma tank modeling and comparison to measurements," *IEEE Trans. Plasma Sci.*, vol. 36, no. 5, pp. 2369–2377, Oct. 2008.

Jean-Charles Matéo-Vélez received the master's degree in engineering in fluid mechanics from the Ecole Nationale Supérieure d'Electronique, d'Electrotechnique, d'Informatique, d'Hydraulique, et des Télécommunications, Toulouse, France, in 2003, the master's degree in research in fluid dynamics from Toulouse University, Toulouse, in 2003, and the Ph.D. degree in fluid dynamics from SUPAERO (ISAE), Toulouse, in 2006.

Since 2007, he has been a Research Scientist with the Physics Instrumentation Environment Space Department, ONERA-The French Aerospace Laboratory, Toulouse. His research interests include spacecraft charging, lunar dust charging and adhesion, instrumentation for nanosatellites, and numerical modeling of spacecraft-plasma-dust interaction. He is the Principal Investigator of the CROCUS Mission Project on 3U CubeSat.

Dr. Matéo-Vélez is a member of the Spacecraft Plasma Interaction Network in Europe (SPINE). He has served as a Referee for the IEEE TRANSACTIONS ON PLASMA SCIENCE.

François Issac, photograph and biography not available at the time of publication.

Julien Jarrige, photograph and biography not available at the time of publication.

Yoann Bernard-Gardy, photograph and biography not available at the time of publication.

Gaël Murat, photograph and biography not available at the time of publication.

Jean Guérard received the master's degree in electronics from Orsay University, in 1992, and the Ph.D. degree in sensors and signal processing applied to musical acoustics from Pierre & Marie Curie University, in 1998.

He started teaching physics and electrical engineering at the university until 2002. Then, he joined the Physics Instrumentation Environment Space Department, ONERA-The French Aerospace Laboratory, Toulouse, France, as a Research Scientist. His main research interests include the development of several MEMS vibrating inertial sensors. He has been responsible for the design and performance analysis of inertial instruments for space missions. He is now in charge of the CROCUS mission architecture, covering both payload and platform hardware and software.

Denis Payan, photograph and biography not available at the time of publication.